On Radar Detection of EeV Air Showers

P. W. Gorham

Jet Propulsion Laboratory, California Institute of Technology
4800 Oak Grove Drive, Pasadena, CA, 91109

Abstract. Extensive air showers produced by EeV cosmic rays leave a significant ionization trail, which may be detectable by radar reflection, by analogy to the way both meteor and lightning ionization trails are presently observed. Such methods could lead to low-cost detection and characterization of events near and above the GZK cutoff.

I INTRODUCTION

It is now clear that the primary cosmic ray spectrum extends in energy beyond the $\sim 5 \times 10^{19}$ eV Greisen-Zatsepin-Kuzmin (GZK) cutoff expected if the particles are hadronic in nature and due to sources at distances greater than about 50 Mpc, still well within the local supercluster volume, and a small fraction ($\sim 0.1\%$) of the volume of the universe to $z \simeq 3$. To answer the question of the origin of these particles demands much higher statistics than we presently have To achieve this will require either a scaling of present detection techniques to much larger collection areas (and correspondingly higher costs), or development of new cost efficient techniques that are sensitive to much larger areas.

One such possibility, that of detecting the ionization column of extensive air showers (EAS) by radar techniques, has its origin in the suggestion by Blackett & Lovell (1940) [1] that earlier detections in the 1930's of sporadic radio reflections at altitudes of 5-20 km from the troposphere and mesosphere [4,2,3,5] might be attributed to cosmic ray EAS, although at the time both the energies and fluxes of such events were only crudely known. This work appears to have led Lovell to construct a large radio antenna in Great Britain dedicated to this purpose [6]; however, for reasons that are unclear (but possibly due in part to skepticism about electron attachment lifetimes) no EAS radar work with this facility was ever reported. The idea was later re-examined in the early 1960's [7] and a proposed experiment was described [8]; however, no results from this test have appeared in the literature to date.

The present work summarizes a more detailed study [9] reported elsewhere which again investigates the viability of this approach, with the advantage of another 40 years of radar technology development that has taken place in the intervening time.

The conclusion is that, depending somewhat on the details of the lifetime of the electrons in the ionization column, the radar approach could be a very powerful technique for EeV shower detection.

II PROPERTIES OF THE IONIZATION COLUMN

A Electron density

Figures 1- 3 show the properties of the ionization column for horizontal air showers at various energies and altitudes. We have chosen to consider only horizontal showers here since it simplifies the analysis, and such showers are of interest for detection of penetrating primaries (such as neutrinos). The parameters of the showers have been modelled according the Nishima-Kamata-Greisen parameterization [10,11] which is reasonably acurate at these high energies.

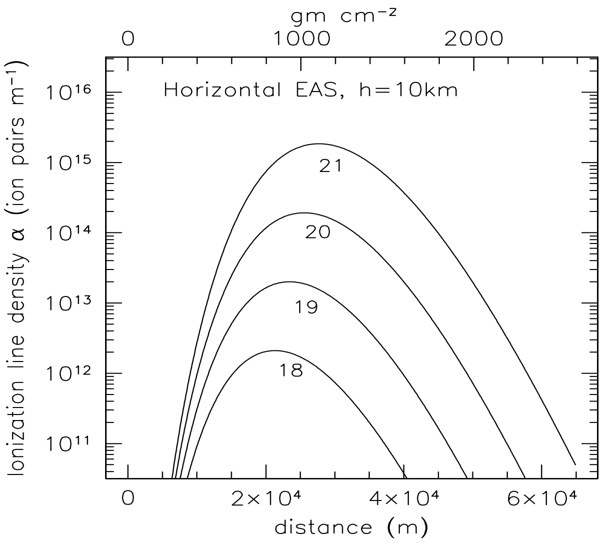

FIGURE 1. Electron ionization line density for 5 showers of energies in the 10^{18} to 10^{21} eV range. Such line densities are quite similar to those of radio meteors.

Fig. 1 shows the profile of the ionization, expressed as line density of electrons (the total number of electrons projected onto the axis of the shower). The free electrons in the ionization column form a tenuous plasma with a radio-frequency index of refraction different from the surrounding neutral atmosphere, and thus there is some reflection of any incident radio waves.

Fig. 2 shows the corresponding electron volume density, along with the plasma frequency ν_p of the ionized region:

$$\nu_p = \sqrt{(n_e e^2/\pi m_e)} \simeq 8.98 \times 10^3 \sqrt{n_e}\ \mathrm{Hz} \qquad (1)$$

where n_e is the electron density in cm^{-3}. If the plasma frequency exceeds the frequency of the incident radiation, the index of refraction becomes imaginary, and total reflection of the incident radiation occurs, rather than refractive scattering.

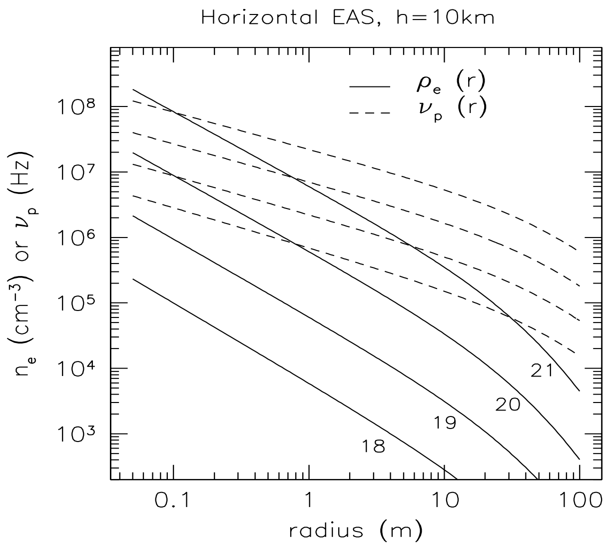

FIGURE 2. Radial dependence of the ionization density for the same showers presented in the previous figure. Also shown is the radial dependence of the plasma frequency for each case.

It is evident that the plasma frequency for this range of energies at 10 km altitude is generally below $\sim$ 10 MHz. This would lead to strong reflections in the MF range (1-10 MHz), which may explain some of the early sporadic detection seen above. However, one drawback of such reflections is that their strength is very sensitive to geometric effects and is not easily interpreted in terms of the amount of ionization present. At higher frequencies, above the plasma frequency, the scattering takes on a much simpler form, depending only on the superposition of the fields from each electron, scattering independently with the Thomson scattering cross section

$$\sigma_T = \frac{8\pi}{3}\left(\frac{e^2}{m_e c^2}\right)^2 \quad = \quad 6.65 \times 10^{-29}\mathrm{m}^2 \ . \tag{2}$$

The total effective radar cross section (RCS) σ_b will then depend on the individual phase factors of each of the scattering electrons [12]:

$$\sigma_b(\mathbf{k}) \quad = \quad \left| \int n_e(\mathbf{r})\sqrt{\sigma_T} e^{2i\mathbf{k}\cdot\mathbf{r}} d^3\mathbf{r} \right|^2 \tag{3}$$

where $\mathbf{k}$ is the wave vector of the incident field ($k = 2\pi/\lambda$), $\mathbf{r}$ is the vector distance to the volume element at which the scattering takes place.

If we now write $\mathbf{q} = 2\mathbf{k}$ equation 3 can be seen to take the form of a Fourier transform, thus reducing the problem of estimating the effective radar cross section to that of calculating the Fourier transform (and the resulting power spectrum) of the electron number density distribution.

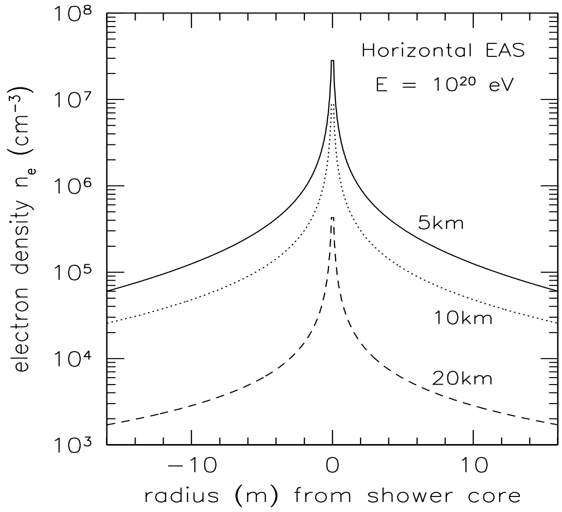

FIGURE 3. Radial profile of showers shown for the inner 40 m radii, plotted on a linear distance scale, for different shower altitudes, showing the effects of altitude for a set of horizontal showers.

A broader implication of this result can be stated as follows: *A measurement of the complex amplitude of the radar echo from an EAS in the underdense case is proportional to a measurement of one Fourier component of the shower ionization profile.* This will be true even in the case of a bistatic radar (receiver location not coincident with transmitter) although there will be an additional coefficient to account for the bistatic cross section and its angular behavior.

B Electron lifetime

The rate of loss to recombination and attachment for atmospheric electrons is described by [13]:

$$\frac{dn_e}{dt} = N_e^0 - \alpha_e n_e^2 - \beta_e n_e \tag{4}$$

where N_e^0, n_e are the initial and evolving electron density, respectively, α_e is the electron-ion recombination coefficient (in units of cm^3 s^{-1}), β_e and is the electron attachment rate (s^{-1}). Direct recombination of the electrons with ions occurs with low probability at the electron densities in air showers, and attachment dominates over recombination. Molecular oxygen is electronegative, forming ions with free electrons primarily through dissociative attachment, via the process

$$\mathrm{e^- + O_2 \rightarrow O^- + O} \tag{5}$$

where the resulting oxygen ion and atom carry off the excess kinetic energy of the electron, and the electron affinity of O_2 is of order 0.5 eV. Molecular nitrogen, in contrast, does not form attachments with electrons but can be more easily collisionally excited, and may play a role in mediating detachment processes in air.

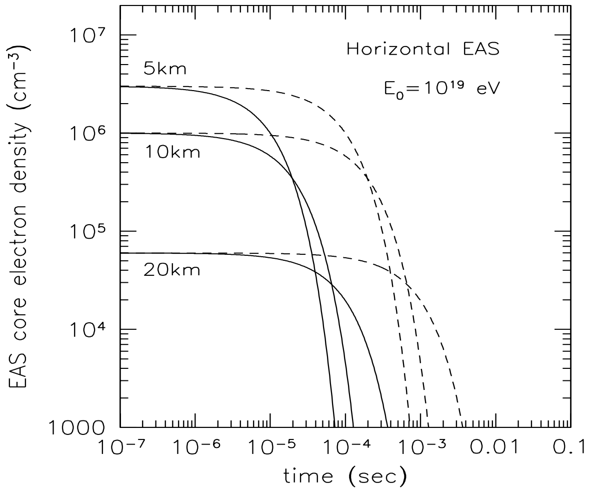

FIGURE 4. The evolution of the electron number density is shown for three 10^{19} eV EAS, at different altitudes. The solid lines correspond to the evolution for the present upper limit on the attachment rate, and the dashed lines to one-tenth of the upper limit.

Several studies of electron attachment in air using electron swarm techniques [14] have indicated a much lower attachment rate than that which is expected from using the attachment coefficient for pure molecular oxygen reduced by the molar ratio in air [15]. Measurements of the attachment coefficient are very sensitive to contamination by carbon dioxide, and CO_2 was not removed from the samples in many early measurements. Although CO_2 can be present in significant concentrations in the near sea level atmosphere, its average concentration in the atmosphere as a whole is 0.033%. Thus electron attachment rates for dry, high-altitude air must be determined with CO_2 largely removed from typical air samples.

Moruzzi & Price (1974) [15], after carefully removing all CO_2 from their samples, confirmed earlier measurements in being unable to detect any attachment in pure dry air. This result was attributed to a competing process: rapid collisional detachment from N_2 interactions, yielding an effective attachment rate that was too small too measure.

Figure 4 shows the behavior of the electron density for three different altitudes for a 10^{19} eV shower core region. Here we have plotted the electron density time evolution for both the case where the attachment rate is equal to the limit of Moruzzi & Price, and one-tenth of the limit (dashed lines). It is evident that the expected electron lifetimes are at least 10-20 μs, increasing slowly at the higher altitudes. Thus, although it is evident that atmospheric conditions may be very important in determining the success of detection of EAS by radar, the lifetime under good conditions should be adequate.[1]

III RADAR CROSS SECTION ESTIMATES

Radar return power P_r is described in terms of a model where the radiation is emitted from an antenna with peak transmitted power P_t and directivity gain $G = 4\pi\Omega_A^{-1}$, where Ω_A is the solid angle of the main beam of the antenna. The radiation is assumed to then scatter from objects in the antenna beam and be re-radiated isotropically in the frame of the scatterer, producing a R^{-4} dependence in the returned power as a function of range R. Deviations from isotropic scattering are thus absorbed into the effective radar backscatter cross-section σ_b, which can be larger or smaller than the physical cross-section of the object. In addition any real transmitting and receiving system will have less than unity efficiency, which we designate here as η. The radar equation under these conditions is [16]:

$$\frac{P_r}{P_t} = \sigma_b \eta \, \frac{G^2 \lambda^2}{(4\pi)^3 R^4} \, . \tag{6}$$

Here we are assuming that the transmitting and receiving antennas are identical, and we are neglecting for the moment any polarization effects or losses in the medium.

Given equation 6, the problem of determining the detectability of EAS-initiated ionization columns reduces to that of determining the effective RCS σ_b for a given choice of operating radar frequency, and the noise power of the specific radar in use. The noise power is given by $P_N = kT_{sys}\Delta f$, where T_{sys} is the system noise temperature, k is Boltzmann's constant, and Δf the effective receiving bandwidth, assumed here to be matched to the transmitting bandwidth.

Combining the noise power equation above with equation 6, the signal-to-noise ratio (SNR) of the received power is

$$\frac{P_r}{P_N} = \sigma_b P_t \eta \, \frac{G^2 \lambda^2}{(4\pi)^3 R^4} \, \frac{1}{kT_{sys}\Delta f} \, . \tag{7}$$

---

1) We note here that this analysis has neglected to treat the 3-body attachment process which may in fact dominate the attachment lifetime if the electrons from the shower thermalize quickly. If the 3-body attachment process is dominant, as appears probable as this article goes to press, then the free electron lifetimes can be much less than for the 2-body process considered here, and may be reduced to several hundred ns. Such short lifetimes will significantly change any approach toward radar detection of air showers. It is thus important to confirm such analysis before settling on a possible experimental approach.

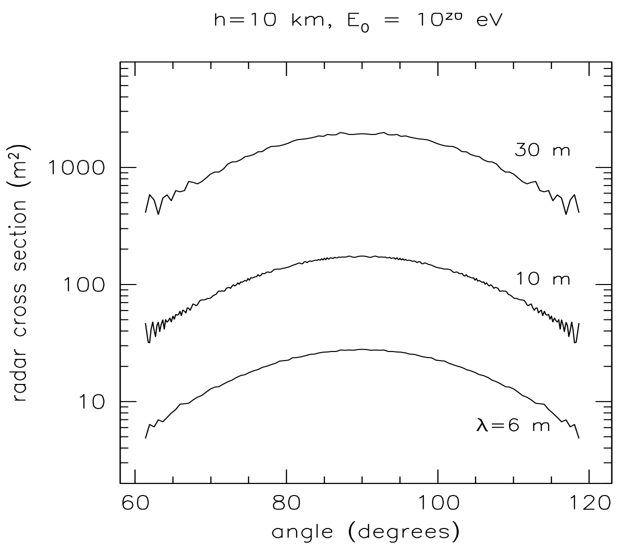

FIGURE 5. Radar cross section over a range of angles centered on normal incidence (at 90°) for a horizontal air shower with $E_0 = 10^{20}$ eV, at an altitude of 10 km, at radar wavelengths 30, 10, and 6 m. Results are based on numerically integrating the contributions of all of the individual volume elements of the shower.

Evaluating equation 7 for a nominal choice of parameters gives the SNR per received radar pulse per square meter of RCS:

$$\frac{S}{N} = 3.3 \left(\frac{\sigma_b}{1\ \mathrm{m}^2}\right) \left(\frac{P_t}{1\ \mathrm{kW}}\right) \left(\frac{\eta}{0.1}\right) \left(\frac{G}{10}\right)^2$$

$$\times \left(\frac{\lambda}{3\ \mathrm{m}}\right)^2 \left(\frac{R}{10^4\ \mathrm{m}}\right)^{-4} \left(\frac{T_{sys}}{10^3\ \mathrm{K}}\right)^{-1} \left(\frac{\Delta t}{10\ \mu\mathrm{s}}\right). \tag{8}$$

We note that the reference values chosen here represent a modest radar system; in particular the peak power of 1 kW is easily attained by current standards, and the directivity $G \simeq 10$ (beam size ~ 1 sr) represents a relatively low-gain antenna. The system temperature $T_{sys} = 1000$ K is realistic for 100 MHz ($\lambda = 3$ m) however, since the brightness temperature of the sky is quite high at these frequencies.

Fig. 5 shows an example of a numerical estimate of the radar cross section for a horizontal 10^{20} eV shower at 10 km altitude, where the effects of individual electron phase factors have been accounted for [9]. It is evident that the cross sections, here peaking at more than 1000 m^2 at 10 MHz, and still several tens of m^2 at 50 MHz, are quite large. Equation 8 indicates that such showers should be detectable out to several tens of km over a reasonable range of incident angles.

IV EXAMPLE OF A POSSIBLE RADAR ARRAY

Because of the issues of antropogenic interference rejection, an EAS radar system would almost certainly have to be constructed with multiple stations configured to both transmit and receive, with pulse encoding such that each station would be sensitive to pulses produced by the other stations. Bistatic radar cross sections of EAS will vary only modestly from the monostatic RCS values treated here. Global synchronization of the stations to several tens of ns or better is routine with the Global Positioning System, particularly with the disabling of Selective Availability (SA) of the high precision GPS codes.

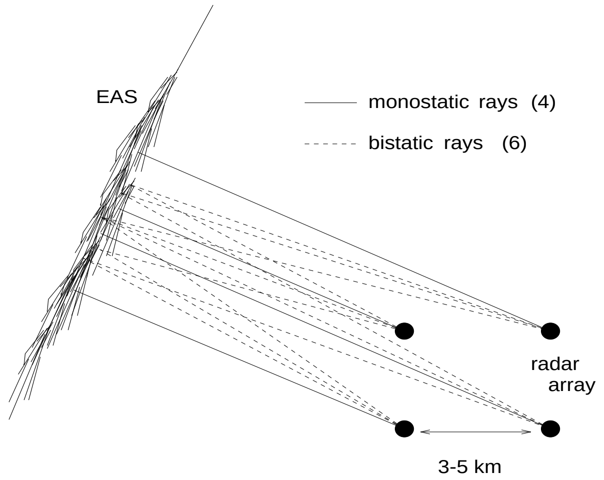

FIGURE 6. An array geometry for a possible standalone EAS radar detection system. Each of the 4 stations has both transmit & receive capability, and can distinguish the signals from the other stations as well.

To optimize the signal-to-noise ratio of the detected echoes, we wish to operate at the lowest frequency that is practical from considerations of background noise, including ionospheric noise from daytime operation. Although lower frequency operation may be possible, we choose here to consider only frequencies above about 30 MHz. In the HF-VHF regime the effective system noise temperature for a remote site (distant from urban noise sources) can be written as [16]:

$$T_{sys} \;=\; 2.9 \times 10^{6} \left(\frac{f}{3 \text{ MHz}} \right)^{-2.9} \quad \text{K} \tag{9}$$

which yields $T_{sys} = 3600\text{K}$ at 30 MHz.

If we assume that we require an energy threshold of 10^{19} eV out to a range of 20 km, the implied RCS for the underdense case is $\sim$ 2 m^2 at this energy. The

TABLE 1. SNR budget for one station of a possible EAS standalone radar system.

Parameter	value	$\pm$dBm
Received Power	$\sigma_b \eta P_t G^2 \lambda^2 \times (4\pi)^{-3} R^{-4}$	
Peak transmit power	60 kW	77.8
Pulse duration	10μs	...
chirp bandwidth	3 MHz	...
Number of repetitions	1	0.0
Antenna gain	3	9.54
wavelength	10 m	20.0
σ_b at $E = 10^{19}$ eV	3.8 m^2	5.8
range to EAS	20 km	-172.0
xmit/rcv efficiency	0.05	-13.0
$(4\pi)^{-3}$	5.04×10^{-4}	-33.0
Received power		-104.9 dBm
Noise power	$kT_{sys}\Delta f$	
Boltmann's constant	1.38×10^{-20}mWK^{-1}Hz^{-1}	-198.6
System temperature	3650 K	35.6
effective bandwidth	100 kHz	50.0
Noise power		-113.0 dBm
Net SNR	6.4	8.0 dB

Fresnel zone length at this range is about 250 m for a shower at 10 km altitude, corresponding to about 10 g cm^{-2} along the track. Using a commercial VHF radar system, it is straightforward to achieve 60 kW peak power and pulse repetition rates of 10-50 kHz for 10 μs pulses. The sky brightness temperature will lead to a system temperature of $T_{sys} = 3600$ K at 30 MHz as noted above. Since we wish to be sensitive to as large a volume as possible, we use an antenna with a broad beam (thus corresponding to a low gain). A suitable system is a vertical monopole or discone system [17] which provides good 2π azimuthal coverage from 5° to about 50° elevation, giving an overall gain of ~ 3 with respect to an isotropic antenna. We also assume here a somewhat pessimistic overall transmit/receive efficiency of $\eta = 0.05$, and a single pulse echo (no pulse averaging) to account for possible rapid decay of the free electron population.

Using these assumptions we show the SNR budget, in dBm (decibels referenced to 1 milliwatt) in Table 1. This budget corresponds to a single monostatic or bistatic pulse measurement in the array. The resulting SNR of 6.4 provides a range resolution of 34 m at a 30 MHz operating frequency, using a chirp bandwidth of 10% (3 MHz in this case).

V CONCLUSIONS

We have investigated the possibility of detecting the ionization column produced by extensive air showers in the 10^{18-21} eV energy range by VHF radar. We have shown that the ionization density is plausibly high enough for such methods, and that the electron lifetimes appear to also be adequate if the air column used for the detection is dry and relatively pure. In this latter respect, higher altitude showers may be more detectable. It is important for tests of this technique to bracket the possible range of electron attachment lifetimes and also to probe higher altitudes where air showers are not normally detected. For example, above 20 km, nearly all fully-developed showers (age ~ 1) are horizontal and may provide good radar targets.

We thank George Resch, David Saltzberg, Elaine Chapin, Ray Jurgens and Tanya Vinogradova for useful discussion and comments. This work was performed in part at the Jet Propulsion Laboratory, California Institute of Technology, under contract with NASA.

REFERENCES

1. Blackett, P. M. S., and Lovell, A. C. B., 1940, Proc. Royal Soc. (London) Ser. A, 177, 183.
2. Watson Watt, R. A., Bainbridge-Bell, L. H., Wilkins, A. F., and Bowen, E. G., 1936, Nature 137, 866.
3. Watson Watt, R. A., Wilkins, A. F., and Bowen, E. G., 1936, Proc. Roy. Soc. A, 161, 181.
4. Colwell, R. C., and Friend, A. W., 1936, Phys. Rev. 50, 632.
5. Appleton, E. V., and Piddington, J. H., 1937, Proc. Roy. Soc. A, 164, 467.
6. T. C. Weekes, this proceedings.
7. Suga K., 1962, Proc. Fifth Interamerican Seminar Cosmic Rays, 2, XLIX.
8. Matano, T., Nagano, M., Suga, K., and Tanahashi, G., 1968, Can. Journ. Phys. 46, S255.
9. P. W. Gorham, 2001, Astroparticle Physics, in press.
10. Kamata, K., & Nishimura, J., 1958, Suppl. Progr. Theoret. Phys. 6, 93.
11. Greisen, K., 1965, in Prog. Cosmic Ray Physics vol. III, J.G. Wilson ed., (North Holland: Amsterdam) 1.
12. Wehner, D. R., 1987, *High Resolution Radar*, (Norwood, MA: Artech House).
13. Thomas, L. 1972, Journ. Atmos. Terr. Phys. 33, 157.
14. Gallagher, J. W., Beaty, E. C., Dutton, J., and Pitchford, L. C., 1983, J. Phys. Chem. Ref. Data, 12(1), 109.
15. Moruzzi and Price (1974).
16. Skolnik, M., 1990, *Radar Handbook*, (New York: McGraw-Hill), 2nd ed.
17. Balanis, C. A., 1997, *Antenna Theory*, 2nd edition, (New York: Wiley & Sons).